RSC Advances

ROYAL SOCIETY OF CHEMISTRY

www.rsc.org/advances

Template confined synthesis of Cu- or Cu_2O- doped SiO_2 aerogels from Cu(II)-containing composites by in-situ alcohothermal reduction

Weiwei Xu, Ai Du, * Jun Tang, Peng Yan, Xiaoguang Li, Zhihua Zhang, Jun Shen, Bin Zhou*

Shanghai Key Laboratory of Special Microstructure Materials and Technology, School of Physics Science and Engineering, Tongji University, Shanghai 200092, P. R. China.

ABSTRACT Uniform and highly dispersed Cu- or Cu_2O- doped SiO_2 aerogels were synthesized via an in-situ alcohothermal reduction strategy. The initial templates with an accurately controllable doping fraction were prepared through a co-gelation method. After alcohothermal reduction and CO_2 supercritical drying, the similar morphology of resulting samples to initial templates was retained. The whole reducing process was systematically studied through a comparative experiment that ethanol, ethylene glycol and glycerol were separately used as reducing agents, and the corresponding converted products were cubic Cu_2O- and Cu-contained silica composites. The specific surface area of the resulting products ranged from 500 to 850 $m^2 \cdot g^{-1}$, and the related microstructure evolution mechanism was comprehensively discussed through the analysis of pore-size distribution. In addition, the high specific surface area and controlled doping amount have made it possible in specific application, such as high efficient photocatalysis and backlight targets.

Key words: In-situ, Alcohothermal reduction, Co-gelation, Controlled doping amount, Backlight targets.

1. INTRODUCTION

The aerogel material assembled by nanoscale colloidal particles or polymer could be recognized as a state of matter rather than as a functional material. [1-2]Among various aerogels, metal and metal-oxide porous materials have received increasing attention in special application, such as gas sensor, electrochemistry, catalysis, thermal insulation and inertial confinement fusion (ICF) targets.[3-9] However, due to the high reactivity and weak crosslinking nature of nanoscale metal particles, it is difficult to prepare a freestanding aerogel which is composed of pure metal.[10] Thus more studies

have been focused on the preparation of metal-doped silica aerogels by adopting both the functionality of the metal and stability of silica networks.[11-16] The general idea is to direct glue the metal or metal oxide particles by using silica sol.[17,18] But due to the influence of gravity, sedimentation could lead to the longitudinal heterogeneity of the final aerogels during gelation and drying process.[19-21] The concentration inhomogeneity results in property inhomogeneity, which may significantly affect their applications. For example, in inertial-confinement fusion experiments (ICF), the distribution of metal particles plays an important role in conversion efficiency of converting laser energy into multi-keV x-rays.[22,23]Thus it is still a problem how to prepare a homogeneous metal- or metal oxide- doped silica aerogels.

In this work, the in-situ alcohothermal reduction method was employed to synthesize homogeneous Cu/SiO_2 composite aerogels with an accurately controllable doping fraction. The Cu(II)-contained silica gel templates were prepared through a propylene oxide pre-reaction method that the Cu(II) compound and silica colloidal particles simultaneously crosslinked into the homogeneous binary gel frameworks. Significantly, the mole ratio of Cu to Si could be accurately controlled and reach as high as 20% via this method. After that, the Cu(II)-contained silica gels were directly reduced by alcohothermal method with different alcohol as a reducing agent. Finally, Cu- or Cu_2O- doped SiO_2 aerogels were obtained after the supercritical fluid drying. According to our knowledge, there has been no related report about the in-situ alcohothermal reduction of metal-based gel in composite networks. In addition, uniform nanoparticles size, high dispersion of the resulting products will not only exhibit a better performance but also provide a quantitative media to study the mechanism in photocatalysis or ICF backlights.

2. EXPERIMENT

Tetramethoxysilane (TMOS), copper chloride ($CuCl_2 \cdot 2H_2O$), 1, 2-epoxy propane (PO, 99.0%), acetonitrile, ethanol, ethylene glycol and glycerol were purchased from Sinopharm Chemical Reagent Co. Ltd., China. All chemicals used in the research are without further purification.

The propylene oxide pre-reaction method was used to synthesize the

Cu(II)-contained silica composite templates according to the following procedure. First, tetramethoxysilane, acetonitrile, deionized water, and propylene oxide with the volume ratio of 1: 1: 0.018: 0.63 were mixed together for pre-reaction. The solution was then poured into another mixture of $CuCl_2 \cdot 2H_2O$ (2.264 g), acetonitrile (20 ml) and water (1.972 ml). Following mixing, propylene oxide (3ml) was added into the mixed solution, and allowed to stir for several minutes. Finally, the homogeneous dark-green gels were obtained after sufficient hydrolysis and condensation of precursors within 30 min at 35 ℃. The wet gels were aged for at least 48 h and then sealed together with 35 ml of reducing agent in a Teflon-lined stainless-steel autoclave (50 ml). The autoclave was heated to 200 ℃ with a speed of 1℃/min, dwelling for 10 h and natural cooling. The resulting products were washed with ethanol for several times, and then dried with CO_2 supercritical drying. In order to systematically study the whole reducing process, ethanol, ethylene glycol and glycerol were separately used as reducing agents. In this paper, the initial aerogel templates and corresponding products reduced by ethanol, ethylene glycol and glycerol were marked as AG-1, AG-2, AG-3, and AG-3, respectively.

The surface morphologies of the samples were examined by a scanning electron microscope (SEM, Philips-XL30), which is additionally equipped with an energy dispersive X-ray spectrometer (EDS). High-resolution transmission electron microscope (TEM, JEOL JEM-2010) was used to characterize the microstructure. The components and crystal structure of resulting products were detected by X-ray diffraction (XRD, Rigaku D/Max-RB). The specific surface area and pore structure parameters of the aerogels were obtained from nitrogen sorption isotherms tested at 77K using a Quantachrome Autosorb-1 analyzer. The Brunauer-Emmett-Teller (BET) and Barrett-Joyner-Halenda (BJH) methods were respectively used to calculate the specific surface area and pore size distribution.

3. RESULTS AND DISCUSSIONS

3.1 The formation mechanisms of Cu(II)-contained SiO_2 gels

The whole experiment process is shown in Scheme 1. Acetonitrile rather than

ethanol was selected as the solvent because the ethanol system exhibits not only a mismatch of gelation time between the two precursors, but also much larger shrinkage during the ageing and drying processes. It could be explained as the discrepancy between different solvents in polarity and coordination effect.[24-26] As a strong polarity solvent, acetonitrile exhibited more significant solvent effect than that of ethanol. That is to say the nitrile group partly replaced the coordinated H_2O on $[Cu(H_2O)_n(OH)_{x-n}]^{2+}$ ($x \leqslant 6$), which stabilized the copper component reactants and as a result slow down the condensation rate to some tent. Due to the fact that acetonitrile is a highly polar aprotic solvent which does not form hydrogen bonds with the silicate nucleophile, so the hydrolysis rate of TMOS could be significantly accelerated comparing with ethanol solvent system.[27,28] In addition, a propylene oxide pre-reaction method was employed during the reaction process of TMOS solution, which had partly improved the hydrolysis extent. Therefore, the reaction rate was balanced between two different precursors, which was benefit for the formation of homogeneous Cu(II)/SiO_2 binary networks.

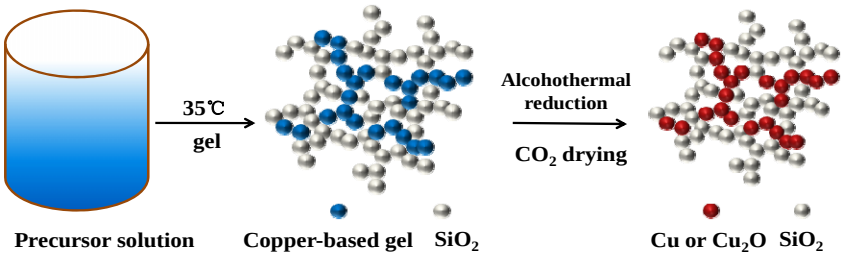

Scheme 1. Schematic of the formation of Cu(II)-contained silica gels and subsequent alcohothermal reduction process.

As shown in the following equation, a similar ring-openinging addition reaction of the propylene oxide is conducted in different precursor solution. In this reaction, PO acts as an irreversible proton capture agent, and two products are generated with similar chemistry structural formula.

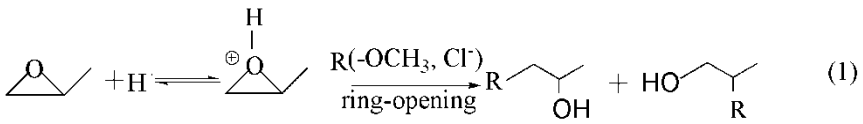

(1)

In TMOS system, H^+ was the hydrolysis product of TMOS and then combined with the oxygen atoms on the epoxy group. Due to the instability of hydroxylating

carbon-oxygen ring, the ring-openinging reaction and subsequent nucleophilic addition process of methoxyl group easily occurred, which partly accelerated the formation of silica gel network.[29] Notable is that the hydrolysis product -OCH_3 exhibited weak electronegativity and the solution was in acidic environment, so the ring-opening addition reaction tended to take place with the alkoxyalcohol product mainly being the second item.[30,31] When the two solutions were mixed together, there was a similar reaction on PO and hydrogen halide, which produced by hydrolysis of $[Cu(H_2O)_n(OH)_{x-n}]^{2+}$. However, the strong electronegativity of chloride ion made the major reaction tended to generate the chloroalcohol product with the first form of structural formula, as shown in equation (1).[32] Homogeneous and coherently supporting binary gel with randomly interconnected networks was obtained through as mentioned co-gelation process.

3.2 Conversion of Cu(II)-contained silica gels into Cu_2O- or Cu-doped SiO_2 aerogels

The main oxidation-reduction reaction is shown in equation 2 (x=1, 2). During the alcohothermal process, the Cu(II)-contained gel skeletons were gradually reduced by the hydroxyl groups in the alcohols, which were then converted to the aldehyde or carbonyl derivatives. [33,34]

$$x/2\ R\text{-}CH_2OH + Cu^{2+} \xrightarrow[\text{alcohothermal}]{200^{\circ}C} Cu^{2-x} + x/2\ R\text{-}CHO + xH^{+} \quad (2)$$

Fig. 1. Photographs of the samples: (a) Cu(II)-contained silica composite gels (left 1) and different reduction products; (b) the corresponding aerogels after CO_2 drying.

As shown in Fig. 1, the macroscopic difference of resulting products is apparent. From the left to right, the samples with separate density of 230 mg·cm^{-3}, 340 mg·cm^{-3},

263.6 mg·cm^{-3}, 237.7 mg·cm^{-3} are respectively initial aerogels (blue, AG-1) and corresponding reducing products of ethanol (yellow, AG-2), ethylene glycol (dark red, AG-3) and glycerol (brick red, AG-4) that based on the solvothermal method. Distinctly, the gels had different shrinkage during the whole process, which could be explained as follows. On the one hand, Cu(II) component may recombine under high-temperature and high-pressure condition. On the other hand, the damage of the capillary forces to the porous structure was unavoidable during the drying process. In addition, the reaction between Cu(II) particles and alcohols reducing agent is a complex process. Whether the monolithic structure could be reserved is mainly determined by the tolerance of the silica frameworks for the alcohothermal process.

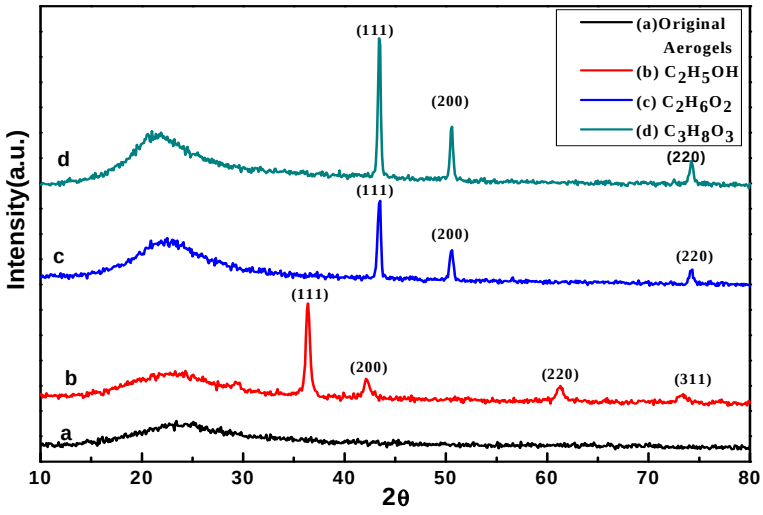

Fig. 2. XRD patterns of composite aerogels: (a) Cu(II)-contained silica composites, and related products with different reducing agent: (b) ethanol, (c) ethylene glycol, (d) glycerol.

In order to analyze the crystal phase composition of Cu(II)-contained silica composites and the converted products, the X-ray diffraction (XRD) patterns were demonstrated in Fig. 2. The initial composite aerogels (Fig. 2a) exhibited a broad diffraction peak around 22°, which was associated with amorphous silica and appeared in subsequent diffraction curves (Fig. 2b, 2c, 2d). After ethanol-thermal reduction, obvious diffraction peaks (Fig. 2b) at 2θ values of 29.6°, 36.5°, 42.3°, 61.5° and 73.4° were present as cubic Cu_2O phase (PDF#075-4299). When ethylene glycol and glycerol were used as reducing agent, the similar diffraction peaks appeared at

43.3°, 50.4° and 74.1° were indexed as the (111), (200) and (220) diffraction of cubic Cu (PDF#04-0836). By contrast, the peak intensity in Fig. 2d is stronger than that in Fig. 2c, which revealed that the copper nanoparticles in glycerol system exhibit a higher crystalline than that of ethylene glycol under the same condition. In addition, the average crystal grain size was estimated from the XRD patterns by using Jade software with the Scherrer equation,[35] and the related value were 9.9 nm (Fig. 2c) and 22.4 nm (Fig. 2d) respectively, which was consistent with the TEM results.

3.3 Morphology and microstructure analysis

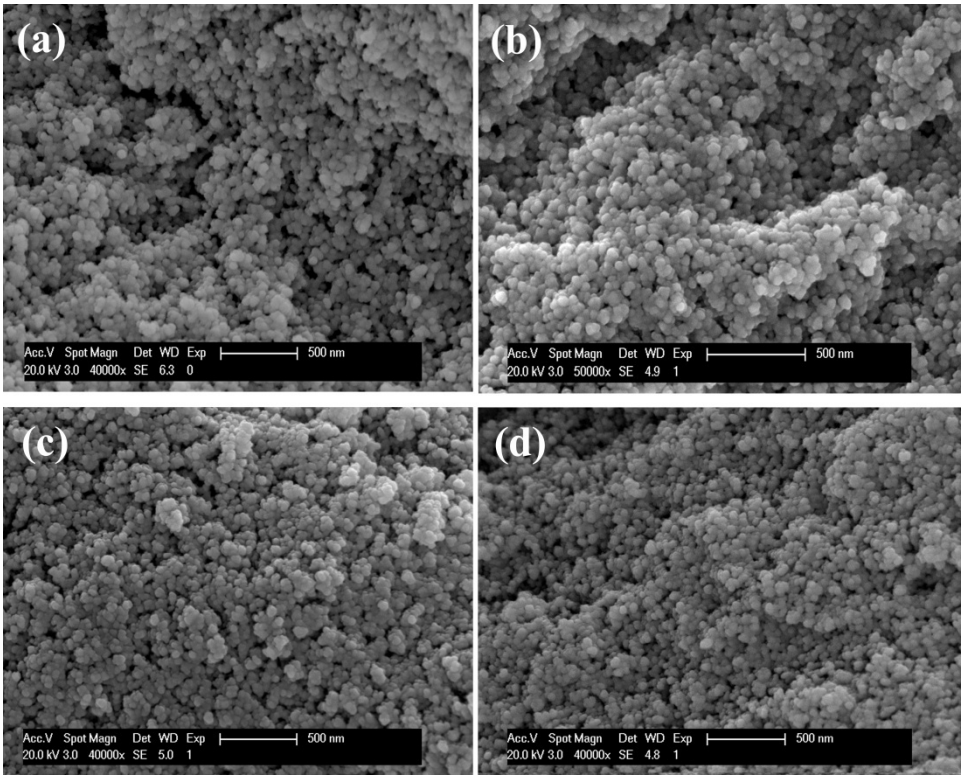

Fig. 3. The SEM images of the resulting aerogels: (a) Cu(II)-contained silica composites; (b) after ethanol reduction; (c) after ethylene glycol reduction; (d) after glycerol reduction.

SEM analyses of the resulting composites were characterized using scanning electron microscopy (SEM). As shown in Fig. 3a, the initial Cu(II)-contained silica composite aerogels exhibited a typical three-dimensional disordered porous framework, which was assembled by uniform primary spherical particles with the diameter about 10-50 nm. The porous structure was preserved after alcohothermal reduction, while partial aggregation of nanoparticles was observed from Fig. 3b to 3d. Meanwhile, the pore structure was slightly collapsed due to the recombination of

Cu(II) gel network, in which the Cu(II) colloidal particles were converted to Cu or Cu_2O nanocrystals under reducing condition. As shown from Fig. S2 to Fig. S5, the molar ratio (n_{Cu} :n_{Si}) of initial templates was about 19.91%±2.42% through statistics of different points using EDS method, indicating that Cu(II) component homogeneously distributed in the whole frameworks. During the subsequent in-situ alcohothermal reduction process, the loss of copper element was inevitable under the high temperature condition. The doping fractions of the resulting aerogels reduced by ethanol, ethylene glycol and glycerol were around 18.6%, 17.8% and 13.8%, respectively (Table 1). In addition, the ratio discrepancy of reduced sample on different points was slight and the doping fraction was relatively high comparing with other doping methods.

Specimen	*Bulk density* ($mg \cdot cm^{-3}$)	*BET* ($m^2 \cdot g^{-1}$)	*Average pore size (nm)*	*Grain size (nm)*	*Doping fraction*
AG-1	230	631	17.5	-	19.91%
AG-2	340	846.4	10.4	8.6	18.6%
AG-3	263.6	722.1	23.09	9.9	17.8%
AG-4	237.7	531.2	19.42	22.4	13.8%

Table 1 The related data of initial Cu(II)-contained silica composites and converted aerogels

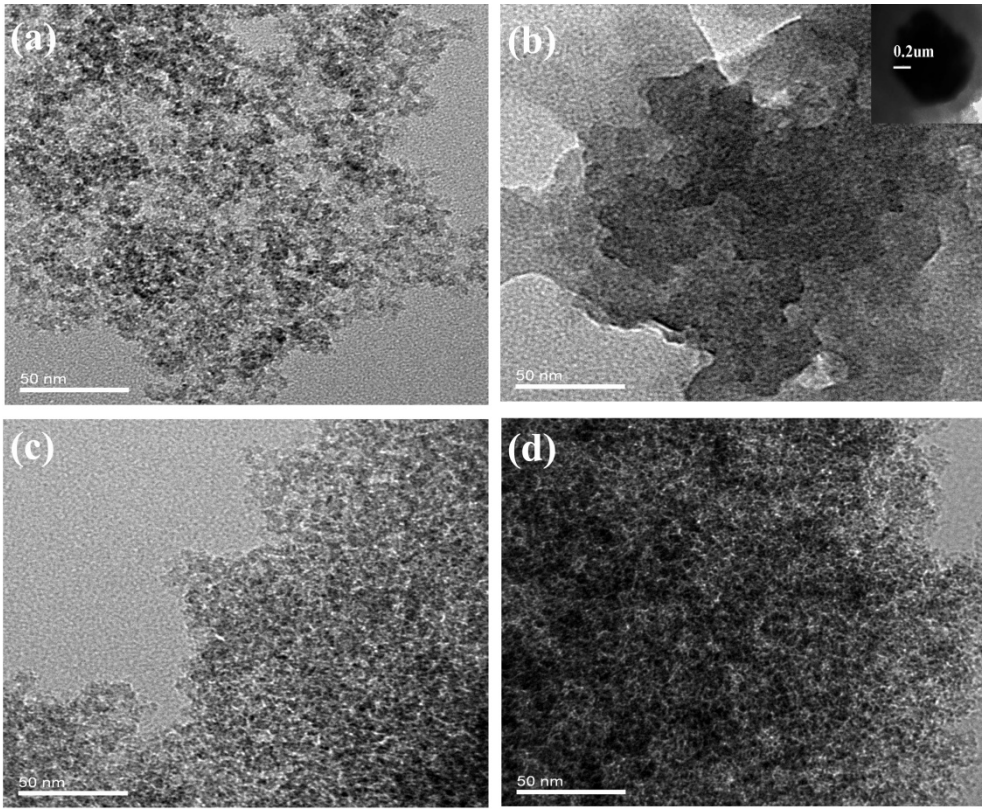

Fig. 4. TEM images of (a) Cu(II)-contained silica composite aerogels and corresponding products with different reducing agents : (b) ethanol, (c) ethylene glycol, and (d) glycerol.

The microstructures of various aerogels were characterized using transmission electron microscopy (TEM). Obviously, these nanocomposites displayed a typical microstructure of common aerogels that nanoparticles clustered together to form a mesoporous structure. As shown in Fig. 4a, the initial aerogels are mainly composed of small spherical particles with a diameter about 1-10 nm, and both the components uniformly dispersed without obvious aggregation of colloidal particles. However, after ethanol-thermal reduction, the shape of the skeleton is similar to randomly distributed root, and some Cu_2O submicron particles were detected in networks, as shown in the Fig. 4b. It could be explained that the nucleation and growth of Cu_2O nanocrystal particles were easily realized under the condition of high-temperature and high-pressure. In contrast, Fig. 4c and Fig. 4d demonstrated that the Cu nanocrystal particles uniformly dispersed in the networks, and aggregation is not obvious in the primary structure. During the reaction process, the framework of Cu(II) component was gradually consumed under reducing condition and the corresponding copper

nanoparticles with a weak interaction were obtained simultaneously. Interestingly, the copper colloidal particles reduced by glycerol have a larger grain size than that with ethylene glycol as the reducing agent, which reveals that glycerol has a stronger reducibility comparing with ethylene glycol.[36,37]

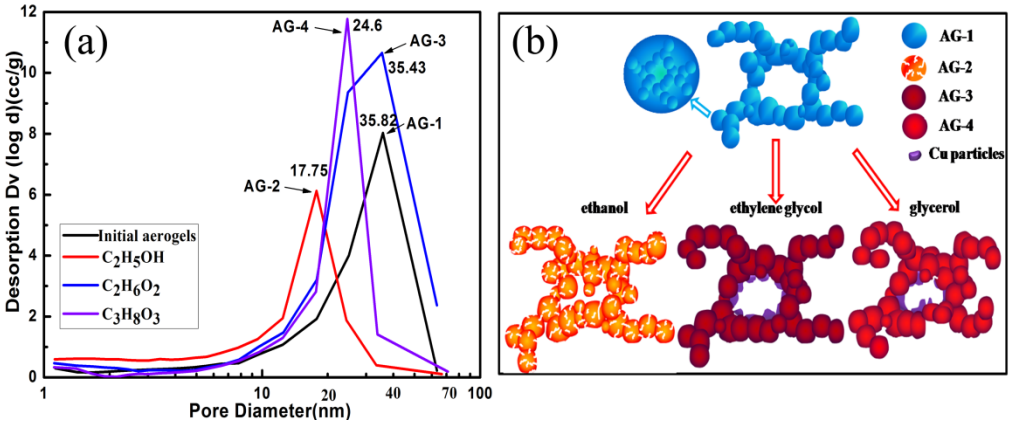

Fig. 5. The distribution and formation mechanism of hierarchical pore of the resulting composite aerogels.

Nitrogen adsorption/desorption isotherms of resulting samples were obtained by Brunauer-Emmett-Teller (BET) method. As described in Fig. S1, the initial aerogels and corresponding samples reduced by ethanol, ethylene glycol and glycerol exhibited similar typical Ⅳ isotherms and narrow H1-type hysteresis loops, which are consistent with the mesoporous structure. The specific surface areas were 631.1 $m^2 \cdot g^{-1}$, 846.4 $m^2 \cdot g^{-1}$, 722.1 $m^2 \cdot g^{-1}$ and 531.2 $m^2 \cdot g^{-1}$, respectively. In addition, the Fig. 5a showed the corresponding cumulative pore volumes and size distribution calculated from the desorption branch of the isotherm applying BJH theory. The initial Cu(II)-contained silica aerogels exhibited a broad pore size distribution mainly in the mesopore range (10-50 nm), which represented the typical characterization of most mesoporous aerogel materials. After an ethanol-thermal process, some micropores ($\leqslant$2 nm) that giving rise to surface area appeared.[38] Meanwhile the main-peak value of mesopore transformed from 35.82 nm down to 17.75 nm comparing with sample AG-1. The change of pore size distribution could be reasonably explained with two factor: (1) the generated micropores were mostly attributed to the in-stiu pore-fabrication during the conversion process from Cu(II) to

Cu_2O component; (2) the shift of main-peak position was mainly caused by the obvious shrinkage of the obtained wet gels during supercritical drying with unavoidable capillary forces, which could be visibly certified from the related photographs of ethanol-reduced wet gels and final aerogels in Fig. 1. As for sample AG-3, a similar pore-size distribution with the initial ones was presented in Fig. 5a. The main peak was still kept at the value about 35nm, while additional sub-peak at 24 nm was appeared after ethylene glycol-thermal reduction. Interestingly, we could found that the pore-size distribution of sample AG-4 exhibited a narrower distribution, and the peak value dropped down to 24.6 nm, which was approximate with the sub-peak of AG-3. According to the as-described change of pore-size distribution, it could be explained that the reaction could mildly take place when ethylene glycol was used as a reducing agent, and the colloidal frameworks could essentially undergo the internal stress, so the reduced sample exhibited the similar pore-size distribution of initial templates. As for the generation of some small mesopores, except for inevitable bulk shrinkage during CO_2 supercritical drying, it mostly attributed to the filling and further fusion effect of the converted copper nanoparticles that the initial pores were partly filled with the primary copper nanoparticles, which then gradually fused into larger size ones. In contrast, the glycol has provided a stronger reducing condition for initial templates, and the reduced copper nanocrystal particles in existing mesopores easily aggregated to larger ones. More importantly, the colloidal skeletons could hardly undergo the internal stress that caused by the reaction between Cu(II) compound and glycerol, and then the composite frameworks partly shrunk even collapsed to varying degrees, as the mechanism described in Fig. 5b. Consequently, this reaction condition could not only result in the macroscopic shrinkage of monolith but also lead to the decrease of specific surface area.

4. CONCLUSION

An in-situ alcohothermal reduction strategy was successfully used to synthesize the highly dispersed Cu- or Cu_2O- doped SiO_2 composite aerogels. The rapid preparation of initial Cu(II)-contained silica templates was attributed to the

employment of both PO pre-reaction and acetonitrile solvent but in different ways. After the alcohothermal reaction with ethanol, ethylene glycol, and glycerol separately as a reducing agent, the resulting Cu_2O/SiO_2 and Cu/SiO_2 composite aerogels could retain some unique properties of the initial templates, such as monolithic appearance, high surface area and nanoscale porous framework. By the analysis of crystal phase composition and pore-size distribution, we could make the conclusion that the reducibility enhanced with the increasing number of -OH on alcoholic molecules under the same condition. Because of uniform nanoparticles size and high dispersion, the resulting products could make it possible in specific application, such as high efficient photocatalysis, and backlight targets.

ACKNOWLEDGMENTS

This work was supported by the National Natural Science Foundation of China (51102184, 51172163), National High Technology Research and Development Program of China (2013AA031801), National Key Technology Research and Development Program of China (2013BAJ01B01), Shanghai Municipal Science and Technology Commission Nano Special Project, China (12nm0503001, 11nm0501600), and Science and Technology Innovation Fund of Shanghai Aerospace, China (SAST201254, SAST201321).

REFERENCE

(1) A. Du, B. Zhou, Z. H. Zhang and J. Shen, *Materials.* 2013, **6**, 941-968.
(2) A. E. Gash, T. M. Tillotson, J. H. Satcher Jr, J. F. Poco, L. W. Hrubesh and R. L. Simpson, *J. Non-Cryst. Solids.* 2001, **285**, 22-28.
(3) J. S. Lee, T. J. Ha, M. H. Hong and H. H. Park, *Thin Solid Films.* 2013, **529,** 98–102.
(4) Y. P. Liu, K. Huang, H. Luo, H. X. Li, X. Qi and J. X. Zhong, *RSC Adv.*, 2014, **4**, 17653–17659.
(5) X. Z. Guo, L. Q. Yan, H. Yang, J. Li, C. Y. Li and X. B. Cai, *Phys.-Chim. Sin.* 2011, **27**, 2478-2484.
(6) H. B. Ren, L. Zhang, C. W. Shang, X. Wang and Y. T. Bi, *J Sol-Gel Sci Technol.* 2010, **53**, 307-311.

(7) G. Q. Zu, J. Shen, L. P. Zou, W. Q. Wang, Y. Lian, Z. H. Zhang and A. Du, *Chem. Mater.* 2013, **25**, 4757-4764.
(8) Z. H. Zhou, X. X. Zhang, C. H. Lu, L. Lan and G. P. Yuan, *RSC Adv.*, 2014, **4**, 8966–8972.
(9) Y. Tokudome, K. Nakanishi, K. Kanamori, K. Fujita, H. Akamatsu and T. Hanada, *J. Colloid Interface Sci.* 2009, **338**, 506-513.
(10) A. K. Herrmann, P. Formanek, L. Borchardt, M. Klose, L. Giebeler, J. Eckert, S. Kaskel, N. Gaponik and A. Eychmuller, *Chem. Mater.* 2014, **26**, 1074-1083.
(11) Y. Q. Zhao, H. L. Zhao, Y. H. Liang, Q. Y. Jia and B. B. Zhang, *Trans. Nonferrous Met. Soc. China.* 2010, **20**, 1463−1469.
(12) Z. Ulker, I. Erucar, S. Keskin and C. Erkey, *Microporous Mesoporous Mater.* 2013, **170**, 353-358.
(13) T. Kristiansen, J. A. Stoeneng, M. A. Einarsrud, D. G. Nicholson and K. Mathisen, *J. Phys. Chem. C.* 2012, **116**, 20368-20379.
(14) J. X. Liu, F. Shi, L. N. Bai, X. Feng, X. K. Wang and L. Bao, *J. Sol-Gel Sci. Technol.* 2014, **69**, 93-101.
(15) H. Z. Guo, X. Liu, Q. S. Xie, L. Wang, D. L. Peng, P. S. Branco and M. B. Gawande, *RSC Adv.*, 2013, **3**, 19812–19815.
(16) J. Tang, A. Du, W. W. Xu, G. W. Liu, Z. H. Zhang, J. Shen and B. Zhou, *J. Sol-Gel Sci. Technol. 2*013**, 68**, 102-109.
(17) W. N. Zhang, J. L. Lu, J. W. Zhu and W. B. Cui, *Asian J. Chem.* 2013, **25**, 877-879.
(18) C. A. Morris, M. L. Anderson, R. M. Stroud, C. I. Merzbacher and D. R. Rolison, *Science.* 1999, **284**, 621-624.
(19) P. R. Aravind, P. Mukundan, P. K. Pillai and K. G. K. Warrier, *Microporous Mesoporous Mater.* 2006, **96**, 14-20.
(20) K. Brodzik, J. Walendziewski, M. Stolarski, L. V. Ginneken, K. Elst and V. Meynen, *J. Porous Mater.* 2008, **15**, 541-549.
(21) K. Grosse, L. Ratke and B. Feuerbacher, *Phys. Rev. B: Condens. Matter.* 1997, **55**, 2897-2902.
(22) K. B. Fournier, J. H. Satcher, M. J. May, J. F. Poco, C. M. Sorce, J. D. Colvin, S. B. Hansen, S. A. MacLaren, S. J. Moon, J. F. Davis, F. Girard, B. Villette, M. Primout, D. Babonneau, C. A. Coverdale and D. E. Beutler, *Phys. Plasmas.* 2009, **16**, 052703/1-052703/13.
(23) K. B. Fournier, C. Constantin, J. Poco, M. C. Miller, C. A. Back, L. J. Suter, J. Satcher, J. Davis and J. Grun, *Physical Review Letters,* 2004, **5196**, 194-204.
(24) P. D. Brown, S. K. Gill and L. J. Hope-weeks, *J. Mater. Chem.* 2011, **21**, 4204-4208.
(25) P. Brown, D. U. Cearnaigh, E. K. Fung and L. J. Hope-weeks, *J Sol-Gel Sci Technol.* 2012, **61**, 104-111.
(26) O. Malay, I. Yilgor and Y. Z. Menceloglu, *J Sol-Gel Sci Technol.* 2013, **67**, 351-361.
(27) I. Artaki, T. W. Zerda and J. Jonas, *Mater. Lett.* 1985, **3**, 493-496.
(28) I. Artaki, T. W. Zerda and J. Jonas, *J. Non-Cryst. Solids.* 1986, **81**, 381-395.

(29) W. Y. Zhang, H. Wang, Q. B. Li, Q. N. Dong, N. Zhao, W. Wei and Y. H. Sun, *Appl. Catal., A.* 2005, **294**, 188-196.
(30) M. N. Timofeeva, V. N. Panchenko, A. Gil, Y. A. Chesalov, T. P. Sorokina and V. A. Likholobov, *Appl. Catal., B,* 2011, **102**, 433-440.
(31) R. E. Parker and N. S. Isaacs, *Chem. Rev.* 1959, **59**, 737-799.
(32) A. Du, B. Zhou, W. W. Xu, Q. J. Yu, Y. Shen, Z. H. Zhang, J. Shen and G. M. Wu, *Langmuir,* 2013, **29**, 11208-11216.
(33) B. Zhou, H. X. Wang, Z. G. Liu, Y. Q. Yang, X. Q. Huang, Z. Lu, Y. Sui and W. H. Su, *Mater. Chem. Phys.* 2011, **126**, 847-852.
(34) J. M. Du, B. X. Han, Z. M. Liu and Y. Q. Liu, *Cryst. Growth Des.* 2007, **7**, 900-904.
(35) A. L. Patterson, *Phys. Rev.* 1939, **56**, 978-982.
(36) X. Y. Chen, X. Wang, Z. H. Wang, J. X. Wan, J. L. Liu and Y. T. Qian, *Nanotechnology.* 2004, **15**, 1685-1687.
(37) H. Tuysuz, Y. Liu, C. Weidenthaler and F. Schuth, *J. Am. Chem. Soc.* 2008, **130**, 14108-14110.
(38) D. J. Suh and T. J. Park, *Chem. Mater.* 1996, **8**, 509-513.